

Coexistence of one- and two-dimensional supramolecular assemblies of terephthalic acid on Pd(111) due to self-limiting deprotonation

M. E. Cañas-Ventura,^{a,b)} F. Klappenberger,^{a,c)} S. Clair,^{d)} S. Pons,^{e)}
K. Kern,^{f)} and H. Brune

*Institut de Physique des Nanostructures, Ecole Polytechnique Fédérale de Lausanne,
CH-1015 Lausanne, Switzerland*

T. Strunskus and Ch. Wöll

Lehrstuhl für Physikalische Chemie I, Ruhr-Universität Bochum, D-44780 Bochum, Germany

R. Fasel

*Empa, Swiss Federal Laboratories for Materials Testing and Research, Nanotech@surfaces Laboratory,
CH-3602 Thun, Switzerland*

J. V. Barth

*Department of Chemistry, University of British Columbia, BC V6T 1Z4 Vancouver, Canada and
Department of Physics and Astronomy, University of British Columbia, BC V6T 1Z4 Vancouver, Canada*

(Received 18 July 2006; accepted 22 September 2006; published online 10 November 2006)

The adsorption of terephthalic acid [$C_6H_4(COOH)_2$, TPA] on a Pd(111) surface has been investigated by means of scanning tunneling microscopy (STM), x-ray photoelectron spectroscopy, and near-edge x-ray absorption fine structure spectroscopy under ultrahigh vacuum conditions at room temperature. We find the coexistence of one- (1D) and two-dimensional (2D) molecular ordering. Our analysis indicates that the 1D phase consists of intact TPA chains stabilized by a dimerization of the self-complementary carboxyl groups, whereas in the 2D phase, consisting of deprotonated entities, the molecules form lateral ionic hydrogen bonds. The supramolecular growth dynamics and the resulting structures are explained by a self-limiting deprotonation process mediated by the catalytic activity of the Pd surface. Our models for the molecular ordering are supported by molecular mechanics calculations and a simulation of high resolution STM images.

© 2006 American Institute of Physics. [DOI: [10.1063/1.2364478](https://doi.org/10.1063/1.2364478)]

I. INTRODUCTION

The terephthalic acid (TPA) molecule (Fig. 1) has demonstrated its capability to form strong and directional linear hydrogen bonds (H bonds) in bulk.¹⁻⁴ Consequently, it is a versatile molecular linker, notably employed to fabricate highly organized supramolecular systems and metal-organic frameworks (MOFs). It has received considerable attention in the design of three-dimensional (3D) self-assembled porous frameworks stabilized by metal-carboxylate bonds,⁵⁻⁹ as well as in two-dimensional (2D) supramolecular architectures at surfaces.¹⁰⁻¹⁸ When such a building block is adsorbed on a surface, the substrate chemical activity and symmetry have an influence in the final variety of molecular architectures. Furthermore, the carboxyl functional end groups do not only exhibit H bonding by dimerization of

self-complementary carboxyl groups, but other bond motifs can be supported if the species in question is deprotonated and present in its carboxylate state.^{11,12,14,15,19} Therefore, we chose a more reactive substrate than those used in previous adsorption studies. Pd(111) has been intensely investigated in the context of hydrogenation catalysis, electrolysis, and hydrogen purification.²⁰ This metal surface acts as a catalyst for the dissociation of H_2 molecules into H atoms^{21,22} and is capable of storing hydrogen both on the surface²³⁻²⁵ and in the subsurface region.^{26,27} Thus, the affinity of the Pd(111) surface towards hydrogen adsorption can be used as the regulator for the hydrogen transfer process between adsorbed building blocks and the substrate. In other studies with organic molecules on metal surfaces, hydrogen transfer needs to be induced by the tip of a scanning tunneling microscope²⁸ (STM) or by annealing.^{11,29}

In this work we present a study of the molecular organization of TPA molecules on a Pd(111) surface. Local investigations by means of STM were complemented by spatially integrating techniques using a synchrotron radiation source, namely, x-ray photoelectron spectroscopy (XPS) and near-edge x-ray absorption fine structure spectroscopy (NEXAFS). A deprotonation driven phase separation between 2D ribbons and one-dimensional (1D) chains was found. Coverage and temperature dependent studies gave information about the dynamics of the two phases. To our

^{a)} Author to whom correspondence should be addressed.

^{b)} Also at Empa, Swiss Federal Laboratories for Materials Testing and Research, Nanotech@surfaces Laboratory, CH-3602 Thun, Switzerland. Electronic mail: marta.canasventura@empa.ch

^{c)} Electronic mail: florian.klappenberger@epfl.ch

^{d)} Present address: The Institute for Physical and Chemical Research (RIKEN), Wako, Saitama 351-0198, Japan.

^{e)} Present address: Laboratoire de Physique des Matériaux, Université Henri Poincaré, F-54506 Vandœuvre-lès-Nancy, France.

^{f)} Also at Max-Planck-Institut für Festkörperforschung, D-70569 Stuttgart, Germany.

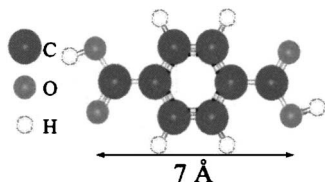


FIG. 1. A 1,4-benzenedicarboxylic acid [terephthalic acid (TPA)] molecule. Atomic positions were calculated by geometry optimization at the AMBER level.

knowledge, TPA chains with a width of a single molecule, which do not rely on a metallic linker¹⁴ and which are stable at room temperature (RT), are reported here for the first time. Our model for the chains is supported by molecular mechanics calculations rationalizing the geometry and by extended Hückel theory (EHT) calculations mimicking the molecular appearance in STM data.

II. EXPERIMENTAL SECTION

The STM experiments were performed in an ultrahigh vacuum (UHV) system (base pressure of 2×10^{-10} mbar) housing sample preparation facilities and a homebuilt low temperature beetle-type STM.³⁰ Images were taken at RT in the constant current mode using a mechanically cut platinum-iridium (Pt-Ir) tip. Indicated voltages for STM images correspond to sample bias. Sample cleaning was performed by cycles of argon ion sputtering ($p_{\text{Ar}} \sim 2 \times 10^{-5}$ mbar, $T=300$ K, $I=7 \mu\text{A}/\text{cm}^2$), annealing at 1000 K in oxygen ($p_{\text{O}_2} < 5 \times 10^{-8}$ mbar), and flash annealing to 1100 K. TPA powder (99+%, Fluka Chemie GmbH) was deposited by organic molecular beam epitaxy (OMBE) from a stainless-steel crucible heated to 450 K onto the crystal kept at 300 K. The sample was then transferred to the STM chamber.

The same Pd(111) crystal was introduced into the UHV system (base pressure of 10^{-9} mbar) of the HE-SGM beamline at the Berlin synchrotron radiation facility BESSY II, where XPS and NEXAFS measurements were carried out. The procedure for sample preparation explained above was similarly employed. The cleanliness of the crystal was checked by XPS on the freshly prepared sample. The widths of the monochromator slits have been set to 200 μm . The XPS data were acquired with a photon energy of 400 eV and a pass energy of the analyzer of 20 eV, providing an energy resolution of ~ 0.7 eV. Data points represent an average of 100 measurements. All spectra were referenced to the Pd $3d_{5/2}$ line at a binding energy (BE) of 335.1 eV. All intensities have been normalized to an average value of the background at 280 eV. A linear background signal has been subtracted from the measured spectra.

The NEXAFS data were recorded in the partial electron yield mode (retarding voltage of 150 V) with a homemade electron detector based on a double channel plate (Galileo) with an energy resolution of ~ 0.35 eV. A carbon-contaminated gold grid provided a characteristic peak (BE of 285 eV) that was registered simultaneously with each spectrum and served as a reference. The raw NEXAFS data have been treated by the following procedure: A constant back-

ground signal, which was present without illumination, was subtracted from all spectra. Then the spectrum of the clean Pd crystal was subtracted from the adlayer spectra. The resulting data was divided by a spectrum of a freshly sputtered gold wafer to compensate the energy dependence of the transmission function of the photon flux. Finally, the intensities were normalized to an edge jump of 1, i.e., the intensity difference between 280 and 330 eV. This processing provides information exclusively on the adsorbed adlayer.

III. RESULTS AND DISCUSSION

A. Morphology and chemical state

The coexistence of two phases of TPA adsorbed on Pd(111), namely, ribbons (α phase) and single molecular lines (β phase) is demonstrated by the STM image in Fig. 2(a), which depicts a sample with ~ 0.3 ML of TPA. 1 ML of TPA corresponds to a fully α phase covered surface. This phase has a molecular adlayer density of 1.93 molecules/ nm^2 . Molecules are resolved as bright spots with an apparent height of $\sim 1.0 \pm 0.1$ Å. The ribbons comprise a quasihexagonal molecular lattice with the primitive translation vectors \vec{a} and \vec{b} (shown in the zoomed part). By averaging the intermolecular distances extracted from several STM images, the lengths of these vectors were found to be $|\vec{a}| = 7.4 \pm 0.4$ Å and $|\vec{b}| = 7.4 \pm 0.8$ Å with an angle of $100^\circ \pm 2^\circ$ in between. From the absence of a modulation in the apparent height of the molecules within the α phase we conclude a commensurate superstructure described in matrix notation by

$$\begin{pmatrix} -3 & 1 \\ 1 & -3 \end{pmatrix},$$

with respect to the substrate unit cell vectors $[01\bar{1}]$ and $[\bar{1}01]$. We define the principal direction of the ribbons, which is seen to be the growth direction, as the one obtained by the sum of \vec{a} and \vec{b} . The intermolecular nearest neighbor distances along the principal direction in the α phase, 9.43 ± 0.37 Å, are almost identical with the nearest neighbor distance in β chains, where we find a value of 9.49 ± 0.59 Å. The inset in the upper right corner shows the atomic lattice of the metal surface and allows the identification of the principal direction of both 1D and 2D structures as $\langle \bar{2}11 \rangle$ Pd(111) directions, i.e., at an angle of 30° to the high symmetry $\langle 1\bar{1}0 \rangle$ directions of the substrate. In a series of images three rotational domains of both phases are found, reflecting the substrate three-fold rotational symmetry. Ribbons oriented along different principal directions do not coalesce even for high coverages.

Figure 2(b) shows a sample with a higher coverage of TPA (~ 0.8 ML). The time interval between sample preparation and molecular deposition (6 h) was about 5 h longer than that for the one presented in Fig. 2(a). As it will be seen later this is important due to the uptake of residual hydrogen. Both phases are clearly distinguishable by their different molecular adlayer densities. The coverage ratio α/β is much lower than in Fig. 2(a). For this sample, a second layer of

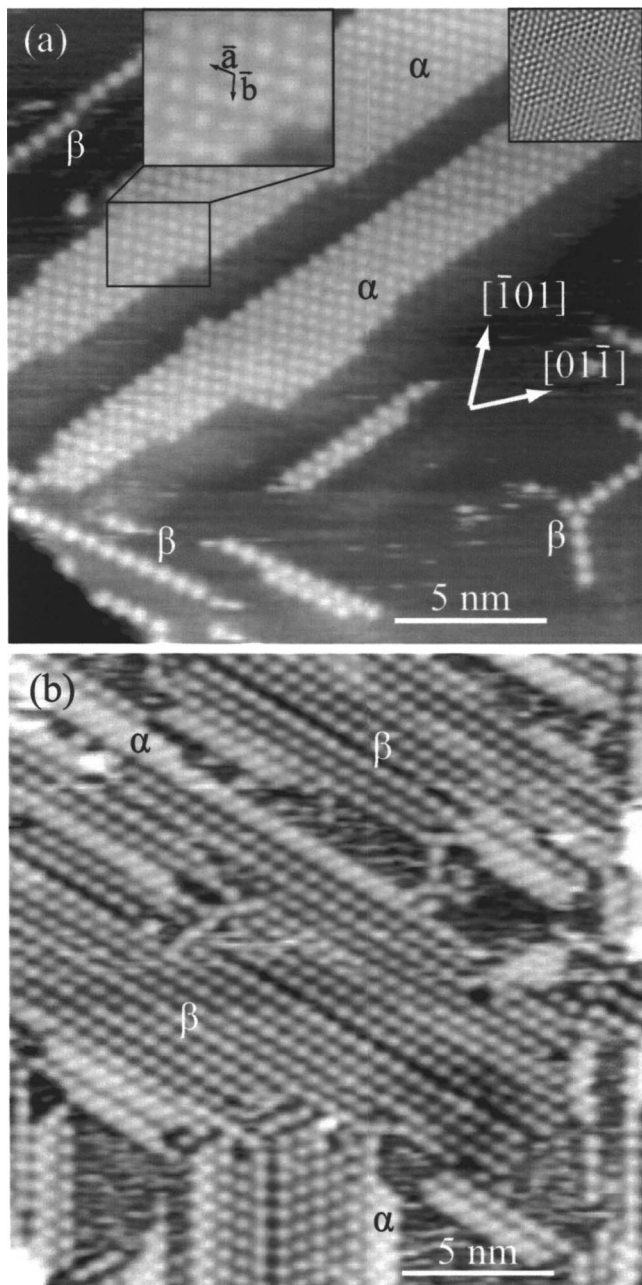


FIG. 2. STM images of TPA deposited on Pd(111) at 300 K, showing the coexistence of a 2D phase (α) and a 1D phase (β). (a) ~ 0.3 ML. The unit cell vectors chosen to describe the molecular structure of the ribbons are shown in the zoom in. Two high symmetry directions $[\bar{1}01]$ and $[01\bar{1}]$ are indicated (image size 31×31 nm², bias voltage $V=420$ mV, tunneling current $I=0.1$ nA, scanned at RT). The inset at the upper right corner shows the atomic resolution of Pd(111) (3×3 nm², $V=13$ mV, $I=1$ nA, scanned at RT). (b) Higher coverage (~ 0.8 ML) of a sample with a time interval in between preparation and molecular deposition longer than that for (a) (31×31 nm², $V=800$ mV, $I=2.6$ nA, scanned at RT).

molecules (not shown) was present in some areas even if there were still some zones of the Pd surface remaining free of TPA molecules.

Figure 3 shows a series of C 1s XPS spectra measured for a sample after deposition of 0.5 ML of TPA (top), after an additional deposition leading to a total coverage of 1.0 ML (middle), and after annealing the 1.0 ML sample to 390 K for 5 min (bottom, discussed in the next section). Both depositions were done with the substrate held at 180 K. The spec-

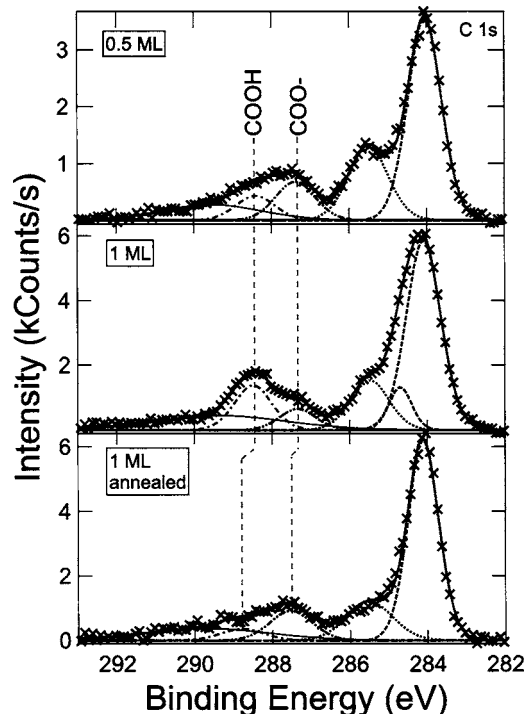


FIG. 3. Photoelectron spectra of the C 1s region for three different TPA adlayers on Pd(111). The experimental data (crosses) have been fitted by a set of Gaussian-Lorentzian lines (dashed). Top: spectrum of a 0.5 ML sample. Middle: spectrum of a 1.0 ML sample, i.e., after adding 0.5 ML to the sample of the upper spectrum. Bottom: spectrum after annealing the 1.0 ML sample at 390 K for 5 min. Carboxyl (COOH) and carboxylate (COO⁻) peak positions are indicated by dashed lines.

tra can be deconvoluted into several peaks, the parameters of which can be found in Table I. The signal at a BE of 285.5 eV is attributed to CO-adsorbed molecules.^{31,32} In an additional experiment, where we cleaned the Pd(111) surface and then only simulated the deposition process by transferring the sample into the preparation chamber with the shutter of the OMBE evaporator closed, a similar CO signature was found. We concluded that, during the deposition process ($p \sim 10^{-8}$ mbar), the Pd(111) surface picks up CO molecules from the residual gas in the preparation chamber. Thus, no indication has been found for dissociation, i.e., the separation of atoms other than the carboxylic hydrogen of TPA molecules on the surface, and we will not further comment on the CO peak from now on. In the 0.5 ML spectrum, when going from low to high BE, sharp peaks with a full width at half maximum (FWHM) of around 1 eV are assigned to C atoms of the phenyl ring (Ph1), of the carboxylate group (COO⁻) and of the carboxyl group (COOH). The broad peak centered at high BE is interpreted as a shake-up peak of the phenyl signal. The COO⁻ entities show an intensity twice that of the COOH entities. The coexistence of two types of molecules is clearly indicated; note that taking into account molecules with only one of the two carboxyl groups deprotonated would give rise to equal intensities for the COOH and the COO⁻ signal. Changing values of the carboxyl/carboxylate peak intensity ratio (from 0.2 up to 0.5) have been found for different samples with a coverage ≤ 0.5 ML. Thus, we attribute the COO⁻ signal to molecules which have

TABLE I. Summary of the parameters for the fitted peaks describing the features in the three C 1s XPS spectra presented in Fig. 3. The binding energy (BE), the assignment, the full width at half maximum (FWHM), and the intensity of each peak are listed.

Sample	BE (eV)	Assignment	FWHM (eV)	Intensity (kcunts/s)
0.5 ML	284.1	Phenyl (Ph1)	1.0	3.9
	285.5	CO	1.2	1.7
	287.4	Carboxylate (COO ⁻)	1.2	0.9
	288.4	Carboxyl (COOH)	1.2	0.6
	289.5	Shake-up	3.0	0.9
1.0 ML	284.1	Phenyl (Ph1)	1.0	6.6
	284.7	Phenyl (Ph2)	0.7	1.0
	285.5	CO	1.2	1.9
	287.3	COO ⁻	1.1	0.8
	288.5	COOH	1.1	1.7
	289.3	Shake-up	4.0	1.9
1.0 ML annealed	284.1	Phenyl (Ph1)	0.9	6.2
	285.5	CO	1.4	1.8
	287.5	COO ⁻	1.3	1.3
	288.8	COOH	1.3	0.5
	289.7	Shake-up	3.9	1.6

lost the H atoms of both carboxyl groups and suggest that the number of fully deprotonated TPA molecules varies from one deposition to another.

After increasing the coverage of the 0.5 ML sample to a full ML (middle spectra in Fig. 3) the following changes were observed. First, the area under the phenyl peak has increased (note the change in the scale), and a second phenyl peak (Ph2) with a slightly higher BE ($\Delta E=0.6$ eV) and a smaller width appears. This peak is attributed to molecules in the second adsorbate layer, since the observed BE is almost the same as that for the phenyl peak of a multilayer sample spectrum (not shown here). Note that our XPS data confirm the STM observation of the second adsorbate layer growth setting for coverages below a full ML. Second, the carboxyl signal is much more intense than before (about five times), while the one from carboxylate remains constant. The evolution of the spectra suggests that the second deposition mainly led to the formation of a nondeprotonated phase. The fact that molecules in the second layer remain protonated indicates that the deprotonation is catalyzed by the substrate and thus limited to the molecules in immediate contact with the Pd(111) surface. In order to determine the ratio of protonated and deprotonated species exclusively in the first monolayer, we subtract a third of the Ph2 peak intensity and obtain that the first monolayer contains almost twice as many protonated as deprotonated molecules.

An XPS study of the O 1s region (not shown) was carried out in addition to the C 1s region. For all samples a single broad peak was found resulting from the convolution of four overlapping peaks stemming from O atoms in the hydroxyl position (C–O–H, BE of 533.9 eV, FWHM of 1.9 eV), in the carbonyl position (C=O, 532.7 eV, 1.9 eV), in the contaminating CO molecules (531.4 eV, 1.9 eV), and from the Pd 3p_{5/2} line (532.4 eV, 3.2 eV). The O 1s data indicated an overall agreement with the results of the carbon

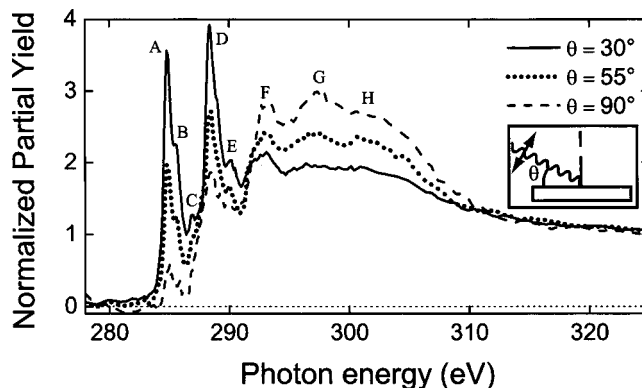


FIG. 4. C *K*-edge NEXAFS spectra for a TPA monolayer adsorbed on a Pd(111) surface. The polarization dependence of the resonances is evidenced by the spectra recorded at grazing ($\theta=30^\circ$), $\theta=55^\circ$, and normal ($\theta=90^\circ$) photon incidence angles. The definition of θ is shown in the inset. Peaks A, B, C, D, and E are associated to C $1s \rightarrow \pi^*$ transitions. F, G, and H correspond to C $1s \rightarrow \sigma^*$ transitions.

region. However, due to the large overlap the amount of the individual species could not be deduced with sufficient precision to provide additional information of physical relevance.

Figure 4 shows a series of carbon *K*-edge NEXAFS spectra of the 1.0 ML sample. Eight peaks have been labeled in the figure: A, B, C, D, and E (at BEs of 284.9, 285.5, 286.8, 288.3, and 290.2 eV, respectively) were assigned to C $1s \rightarrow \pi^*$ transitions and F, G, and H (at BEs of around 293.2, 297.7, and 301 eV, respectively) to C $1s \rightarrow \sigma^*$ transitions.³³ The set of spectra shows a clear θ dependence of the peak intensities. In particular, the pronounced dichroism of peaks A and B, which are related to the phenyl ring, and of peak D, which is connected to the carbonyl group, indicates almost flat lying molecules. To be more precise, the least square deviation fit of the experimental intensities to the theoretical curves for a vector-type π orbital indicates an average tilt angle of $\sim 20^\circ$. For this we took the three-fold substrate symmetry and a polarization of the exciting light of 0.82 into account. Typically, the transition moments related to C $1s \rightarrow \pi^*$ transitions are oriented perpendicular to the molecular plane, defined here as the plane made up of the C atoms of the phenyl ring. In the ideal case, these peaks should vanish completely for $\theta=90^\circ$. In our case of a strongly chemisorbed molecule, however, it is likely that the hydrogen atoms connected to the phenyl ring are bent away from the surface, similar to the case of benzene on Pt(111).^{34,35} Assuming that the H of the benzene were tilted out of the plane by 20° , Mainka *et al.*³⁶ calculated a normal incidence signal of about a tenth of the grazing incidence signal. In addition, molecules at the step edges and at impurity or dislocation sites contribute to the NEXAFS signal and can have a more tilted geometry. Thus, we suggest that the adsorption geometry in the regular monolayer may be much flatter than the 20° deduced from the angular intensity dependence.

In order to understand the mechanism responsible for the coexistence of phases observed in STM images, annealing experiments were performed after molecular deposition at RT. The XPS spectrum in Fig. 3 (bottom) shows that by annealing the 1.0 ML sample for 5 min at 390 K the mol-

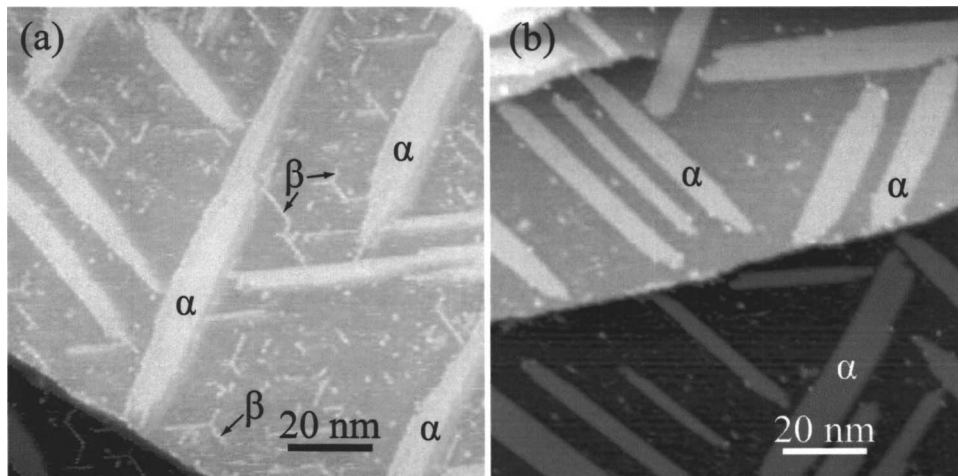


FIG. 5. STM images with similar coverages (~ 0.3 ML) deposited at RT, both scanned at RT and with a size of 113×113 nm². (a) Without annealing, the coexistence of α and β phases can be identified ($V = -80$ mV, $I = 0.14$ nA). (b) After performing a short annealing to 390 K, the β phase coverage is strongly reduced ($V = -1800$ mV, $I = 0.24$ nA).

ecules of the second adlayer are desorbed as indicated by the disappearance of the Ph2 peak. The phenyl area decreases by 20%, from which the minor desorption of first adlayer molecules was deduced. The carboxylate peak shows an intensity almost three times higher than the carboxyl peak, with the BE of both peaks being slightly upshifted ($\Delta E = 0.2\text{--}0.3$ eV). This evolution of the spectra shows that during annealing most of the protonated molecules are transformed into deprotonated entities.

These findings are supported by STM measurements. In Fig. 5 we compare samples without (a) and with (b) a 3 min annealing at 390 K. Before annealing, 1D molecular chains can be identified in the extended areas in between 2D ribbons. However, upon annealing, the β phase almost disappears. STM data with higher resolution than Fig. 5(b), taken from different samples with similar annealing conditions, indicate that, after annealing, residuals of the β phase are still present. As the surface coverage stayed almost the same when annealing, we conclude, first, that the desorption of TPA molecules is negligible up to 390 K, and second, that during the annealing process, the α phase grows at the expense of the β phase.

The NEXAFS spectra of the annealed sample (not shown) present similar features but broader peaks compared to the 1.0 ML sample (Fig. 4). The angular dependence of the peak intensities is almost the same as that without annealing. Taking into account that the β phase almost completely disappears during annealing of the sample, we rule out a scenario where the β phase involves tilted and the α phase flat lying molecules.

B. Models and simulations

Combining STM, XPS, and NEXAFS results, we suggest the following scenario: two phases coexist at the surface. They differ in appearance in STM images and involve different chemical states (carboxyl and carboxylate) as deduced from XPS data. The carboxylate (carboxyl) peak intensities can be related to the α (β) phase involving deprotonated (protonated) molecules. Annealing promotes deprotonation and thus transfers the β into the α phase.

In Figs. 6 and 7, models for the supramolecular structures of each phase are presented. Figure 6(a) shows a high

resolution STM image of an α phase ribbon. The frame indicates the area for which the model is given in Fig. 6(b). Pd(111) surface atoms with a nearest neighbor distance of 2.75 Å are represented by open circles. TPA is drawn to scale with the substrate lattice: its geometrical structure was optimized by molecular mechanics calculations at the AMBER level. The unit cell vectors for the 2D arrangement are indicated, having a length of $|\vec{a}| = |\vec{b}| = 7.3$ Å and an angle of 98° in between. Each TPA molecule binds to four neighboring molecules by means of eight ionic H bonds ($\text{C}-\text{O}^- \cdots \text{H}-\text{C}$, dashed lines in the model). Note that for each of these ionic H bonds the negative charge associated with one O atom is a partial charge. This ordering gives rise to a distance of 2.6 Å in between C and O atoms involved in the ionic H bonds. The center of the molecules are placed on a top site position, which leaves the molecules adsorbed in a completely symmetric environment. The ring sits on the most favorable combination of binding site and orientation as found for benzene on Pd(111).³⁷ All O atoms are adsorbed on bridge sites. The orientation of the molecules within ribbons provides the largest possible separation between charged groups (carboxylates). The geometry of the model agrees well with the intermolecular distances measured by STM. The anisotropic growth of the ribbons can be understood with the help of the following scenario. Let there be a group of molecules ordered in the same way as depicted in Fig. 6(b). A TPA molecule binding along the principal direction is a favorable situation, since it only needs to find the appropriate rotation. However, a TPA molecule binding along the perpendicular direction has to overcome an electrostatic potential barrier due to the charged carboxylate species. Therefore, it is more likely that molecules bind along the principal direction, hence anisotropic growth will take place. With more binding energy available this potential barrier should be easier to overcome. Indeed, for samples with higher coverage than 0.4 ML after annealing at 390 K, supramolecular structures with a length to width aspect ratio much nearer to 1 were observed. This temperature-induced reduction of the anisotropic growth strongly supports our explanation. Another experimental finding, namely, that ribbons with different principal directions do not coalesce, can be explained by symmetry reasons. As the supramolecular structure does not

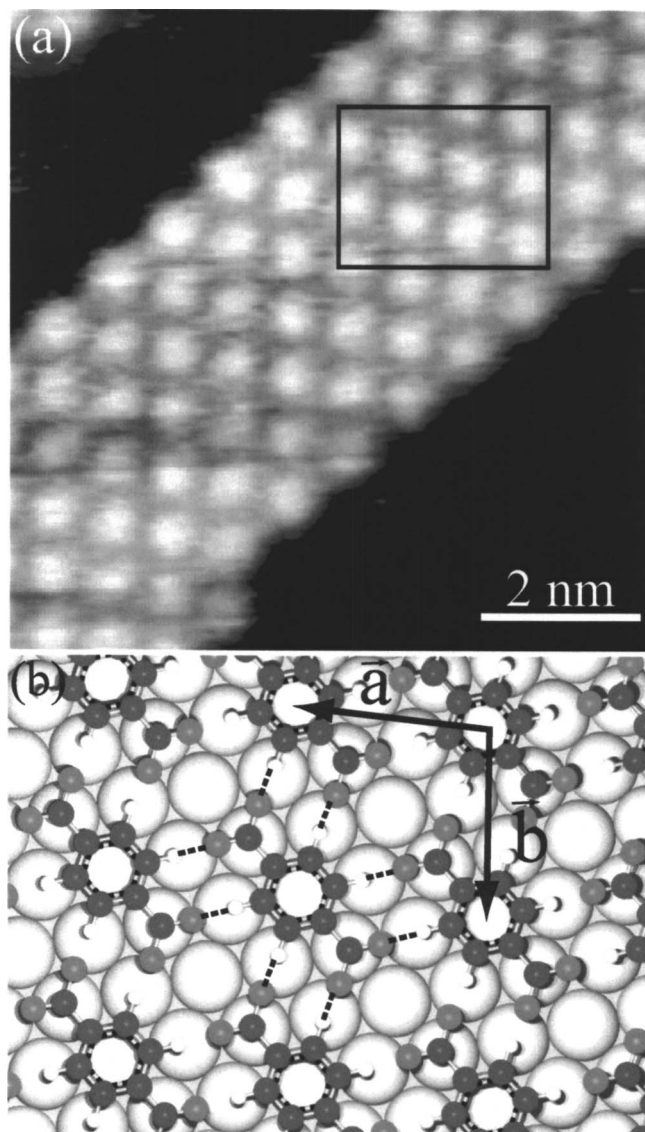


FIG. 6. (a) STM image of an α phase ribbon ($8 \times 8 \text{ nm}^2$, $V=460 \text{ mV}$, $I=0.2 \text{ nA}$). (b) Corresponding schematic drawing for the frame highlighted in (a). Unit cell vectors are drawn. Open circles represent palladium surface atoms. The molecular end groups are deprotonated. Ionic H bonds are indicated by dashed lines. Pd substrate directions are consistently oriented in both figures.

have the three-fold rotational symmetry, molecules within ribbons rotated by 120° are differently oriented and this bonding patterns are not compatible.

The 1D molecular chain model is shown in Fig. 7(b) and corresponds to the β phase segment contoured by the frame in the upper STM image [Fig. 7(a)]. TPA molecules within chains are suggested to be linked along the direction of the chains by two-fold classical H bonds ($\text{C}=\text{O} \cdots \text{H}-\text{O}$, dotted lines in the model). In these bonds the distance between both O atoms is 2.5 \AA , giving rise to an intermolecular distance of 9.5 \AA in good agreement with intermolecular distances measured from STM data ($9.5 \pm 0.6 \text{ \AA}$). Molecular mechanics results using AMBER and confining the TPA molecules in 2D without explicitly considering the Pd surface show that the most stable configuration for dimerized TPA molecules involves a rotation of the molecular axis by 5° with respect to

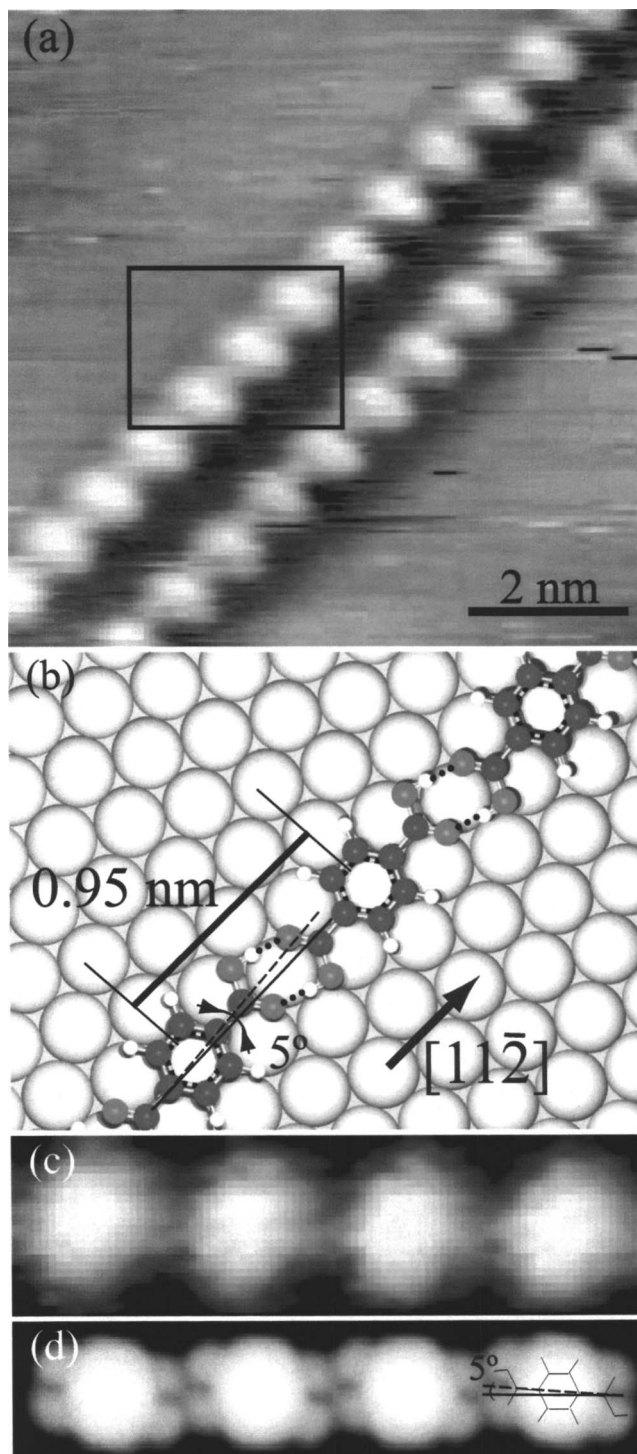


FIG. 7. (a) STM image of two β phase chains ($8 \times 8 \text{ nm}^2$, $V=580 \text{ mV}$, $I=0.5 \text{ nA}$). (b) Corresponding tentative model for the frame in (a). Open circles represent palladium surface atoms. Dotted lines indicate the classical H bonds between molecules. The long molecular axis is tilted by 5° with respect to the $[11\bar{2}]$ chain direction. (c) STM image ($4.0 \times 1.1 \text{ nm}^2$, $V=50 \text{ mV}$, $I=2.2 \text{ nA}$) of four TPA molecules in a 1D chain. In this case the chain has an opposite chirality with respect to the chains in (a). (d) Corresponding STM image simulation using the optimized geometry calculated with AMBER. A schematic drawing of one of the four TPA molecules is superimposed. The 5° tilt of the long axis is indicated.

the chain direction ($[11\bar{2}]$). Chiral properties of the chains follow from the fact that this 5° tilt can appear towards both sides of the chain direction. This configuration, together with the top site position for the center of the molecules, leaves

them in an almost symmetric environment and with carboxylate oxygen atoms adsorbed on bridge sites. In agreement with these results, the elliptical shape of the bright spots within chains [see Figs. 7(a) and 7(c)], is indeed found in all STM images independent of the scanning parameters. The long axis of this ellipse is almost perpendicular to the chain direction. A small deviation from the orthogonal orientation is observed towards both sides of the chain, for all three chain orientations. This is indicative of the chiral chain structure. In Figs. 7(a) and 7(c) STM images of both mirror symmetric configurations are shown. Semiempirical calculations were used to explain such a nonintuitive shape for the TPA STM fingerprint. Sample orbital calculations using EHT were performed and implemented in order to simulate STM images,³⁸ without taking the surface into account. The mimicked constant current STM image in Fig. 7(d) was obtained by the representation of the constant electron density contour resulting from the integration of the 16 occupied molecular orbitals with the highest energies, which are expected to be close to the E_F of the substrate. The resulting gray level intensity plot exhibits a bright maximum at the phenyl ring position. The elliptical shape, with its long axis almost perpendicular to the long axis of the molecule, is seen to originate from the phenyl hydrogen atom positions. With the addition of the surface effect, these H atoms are expected to be somewhat tilted upwards, which might further contribute in highlighting the apparent elliptical shape.

C. Phase selection by a tuning of the self-limiting deprotonation

We understand the deprotonation of TPA molecules as the consequence of the high affinity of the Pd(111) surface towards hydrogen. However, the reactivity of the Pd surface is strongly reduced during the accumulation of H atoms on the surface. Thus the TPA deprotonation is a self-limiting process, itself delivering the H atoms, which lower the chemical activity of the surface and posteriorly stop the deprotonation. During the deposition of molecules onto a clean surface, the first adsorbed molecules deprotonate, which results in the formation of α phase ribbons and in the accumulation of H atoms on the surface. Then, with more arriving molecules, the increasing H surface concentration prevents further deprotonation and induces the formation of β phase chains. For the sample with 0.3 ML coverage [Fig. 2(a)], the end of deprotonation appeared at about 0.25 ML coverage. Assuming a Pd surface free of H atom prior deposition, we calculate the deprotonation blocking coverage of 0.3 H atoms per Pd surface atom.

The high H affinity of the clean Pd(111) surface leads to deprotonation, but it is also the cause for the dissociative adsorption of H_2 from the residual gas in the chamber. Thus, sample preparation, quality of UHV, and time interval in between the end of preparation cycles and molecule exposure are parameters that change the status of the Pd(111) sample at the moment of the molecular deposition. This status influences the final α phase coverage, since it constrains the number of permitted deprotonation events. We estimate that at the base pressure of our UHV chamber,³⁹ the flux of H_2 molecules from the residual gas on the surface is <2.6

$\times 10^{14}$ molecules $m^{-2} s^{-1}$. Assuming a sticking coefficient of 1 and $\sim 23 \text{ \AA}^2/\text{molecule}$, a period of about 5 h would be needed to completely cover the surface with a $\sqrt{3} \times \sqrt{3}$ structure of H atoms.²⁴ We employed this fact to give additional evidence that adsorbed H is blocking the deprotonation. An STM experiment with a sample where ~ 0.1 ML of TPA were deposited 7 h after surface cleaning showed the presence of a $\sqrt{3} \times \sqrt{3}$ structure attributed to chemisorbed H atoms.²⁴ On this sample no α phase could be found, supporting our assumption that a H saturated Pd(111) surface loses its capability to deprotonate the TPA. The adlayer of H atoms prior to molecular deposition is responsible for the α/β coverage ratio. We suggest that by increasing or decreasing the H atom coverage before TPA deposition, in a sufficiently controlled system, one could tune the ratio of 1D and 2D structured phases. The assumption of a H adlayer is also consistent with the fact that multilayer growth starts for TPA coverages <1 ML, which was found in both XPS and STM measurements. As the Pd surface is partially covered with H atoms, the TPA molecules prefer to populate the second layer. The increase of deprotonated species upon annealing is related to the thermal desorption of hydrogen atoms.²³ This desorption reactivates the catalytic capabilities of the Pd surface. In addition, a second channel for deprotonation might become important: protons coming from deprotonation reactions could desorb directly from the system, without being trapped by the Pd surface. Furthermore, the desorption of H atoms from the subsurface to the surface might not be neglectable and should be considered as another factor lowering the catalytic activity of the surface. To our knowledge, the deprotonation of small organic molecules guided by intrinsic properties of the Pd(111) surface at RT is a unique feature of the present system.

IV. CONCLUSION

The adsorbate-substrate and adsorbate-adsorbate interactions of TPA molecules on the Pd(111) surface were investigated with a combination of STM, XPS, and NEXAFS experiments. The coexistence of 1D chains of protonated molecules and 2D ribbons of deprotonated molecules was explained to be the result of a self-limiting deprotonation process: the clean substrate induces deprotonation of TPA entities and accumulates H atoms, which block the catalytic behavior of the Pd surface up to a threshold of 0.3 ML. The amount of preadsorbed H atoms was shown to control the resulting molecular structures.

ACKNOWLEDGMENTS

This work was partially supported by the European Science foundation EUROCORES Programme SONS (as part of the FUN-SMARTs) and the EC Sixth Framework Programme (as part of the STREP BioMACH). The authors thank O. Gröning for providing the software to simulate STM images and BESSY for attribution of beam time. Travelling costs for synchrotron measurements provided by BMBF through Grant No. 05ESXBA/5 are gratefully acknowledged.

- ¹M. Bailey and C. J. Brown, *Acta Crystallogr.* **22**, 387 (1967).
- ²V. S. Korobkov and N. K. Zharikov, *Zh. Prikl. Spektrosk.* **19**, 658 (1973).
- ³H. Fjær and E. J. Samuelsen, *J. Phys. C* **19**, 5945 (1986).
- ⁴M. Slédz, J. Janczak, and R. Kubiak, *J. Mol. Struct.* **595**, 77 (2001).
- ⁵O. M. Yaghi, M. O'Keeffe, N. W. Ockwig, H. K. Chae, M. Eddaoudi, and J. Kim, *Nature (London)* **423**, 705 (2003).
- ⁶G. Férey, C. Mellot-Draznieks, C. Serre, F. Millange, J. Dutour, S. Surblé, and I. Margiolaki, *Science* **309**, 2040 (2005).
- ⁷K. Larsson and L. Öhrström, *CrystEngComm* **6**, 355 (2004).
- ⁸S. H. Dale and M. R. J. Elsegood, *Acta Crystallogr., Sect. C: Cryst. Struct. Commun.* **59**, 475 (2003).
- ⁹X. Mei and C. Wolf, *Eur. J. Org. Chem.* **2004**, 4340 (2004).
- ¹⁰S. Clair, S. Pons, A. P. Seitsonen, H. Brune, K. Kern, and J. V. Barth, *J. Phys. Chem. B* **108**, 14585 (2004).
- ¹¹S. Stepanow, T. Strunskus, M. Lingenfelder, A. Dimitriev, H. Spillmann, N. Lin, J. V. Barth, Ch. Wüll, and K. Kern, *J. Phys. Chem. B* **108**, 19392 (2004).
- ¹²S. Stepanow, M. Lingenfelder, A. Dimitriev, H. Spillmann, E. Delvigne, N. Lin, X. Deng, C. Cai, J. V. Barth, and K. Kern, *Nat. Mater.* **3**, 229 (2004).
- ¹³M. A. Lingenfelder, H. Spillmann, A. Dimitriev, S. Stepanow, N. Lin, J. V. Barth, and K. Kern, *Chem.-Eur. J.* **10**, 1913 (2004).
- ¹⁴S. Clair, S. Pons, H. Brune, K. Kern, and J. V. Barth, *Angew. Chem., Int. Ed.* **44**, 7294 (2005).
- ¹⁵S. Clair, S. Pons, S. Fabris, S. Baroni, H. Brune, K. Kern, and J. V. Barth, *J. Phys. Chem. B* **110**, 5627 (2006).
- ¹⁶A. P. Seitsonen, M. Lingenfelder, H. Spillmann, A. Dimitriev, S. Stepanow, N. Lin, K. Kern, and J. V. Barth, *J. Am. Chem. Soc.* **128**, 5634 (2006).
- ¹⁷J. V. Barth, G. Constantini, and K. Kern, *Nature (London)* **437**, 671 (2005).
- ¹⁸A. Dimitriev, H. Spillmann, N. Lin, J. V. Barth, and K. Kern, *Angew. Chem., Int. Ed.* **42**, 2670 (2003).
- ¹⁹M. W. Hosseini, *Coord. Chem. Rev.* **240**, 157 (2003).
- ²⁰M. Morkel, V. V. Kaichev, G. Rupprechter, H.-J. Freund, I. P. Prosvirin, and V. I. Bukhtiyarov, *J. Phys. Chem. B* **108**, 12955 (2004).
- ²¹N. Lopez, Z. Lodziana, F. Illas, and M. Salmeron, *Phys. Rev. Lett.* **93**, 146103 (2004).
- ²²T. Mitsui, M. K. Rose, E. Fomin, D. F. Ogletree, and M. Salmeron, *Nature (London)* **422**, 705 (2003).
- ²³W. Eberhardt, S. G. Louie, and E. W. Plummer, *Phys. Rev. B* **28**, 465 (1983).
- ²⁴K. Nobuhara, H. Nakanishi, H. Kasai, and A. Okiji, *J. Appl. Phys.* **88**, 6897 (2000).
- ²⁵T. Mitsui, M. K. Rose, E. Fomin, D. F. Ogletree, and M. Salmeron, *Surf. Sci.* **540**, 5 (2003).
- ²⁶M. K. Rose, A. Borg, T. Mitsui, D. F. Ogletree, and M. Salmeron, *J. Chem. Phys.* **115**, 10927 (2001).
- ²⁷E. C. H. Sykes, L. C. Fernández-Torres, S. U. Nanayakkara, B. A. Mantooth, R. M. Nevin, and P. S. Weiss, *Proc. Natl. Acad. Sci. U.S.A.* **102**, 17907 (2005).
- ²⁸B. V. Rao, K.-Y. Kwon, A. Liu, and L. Bartels, *J. Chem. Phys.* **119**, 10879 (2003).
- ²⁹M. Stöhr, M. Wahl, C. H. Galka, T. Riehm, T. A. Jung, and L. H. Gade, *Angew. Chem., Int. Ed.* **117**, 7560 (2005).
- ³⁰S. Clair, Ph.D. thesis, Ecole Polytechnique Fédérale de Lausanne, 2004; available in <http://library.epfl.ch/theses/>
- ³¹V. V. Kaichev, I. P. Prosvirin, V. I. Bukhtiyarov, H. Unterhalt, G. Rupprechter, and H.-J. Freund, *J. Phys. Chem. B* **107**, 3522 (2003).
- ³²V. V. Kaichev, M. Morkel, H. Unterhalt, I. P. Prosvirin, V. I. Bukhtiyarov, G. Rupprechter, and H.-J. Freund, *Surf. Sci.* **566-568**, 1024 (2004).
- ³³T. Okajima, K. Teramoto, R. Mitsumoto, H. Oji, Y. Yamamoto, I. Mori, H. Ishii, Y. Ouchi, and K. Seki, *J. Phys. Chem. A* **102**, 7093 (1998).
- ³⁴S. Lehwald, H. Ibach, and J. E. Demuth, *Surf. Sci.* **78**, 577 (1978).
- ³⁵A. B. Anderson, M. R. McDevitt, and F. L. Urbach, *Surf. Sci.* **146**, 80 (1984).
- ³⁶C. Mainka, P. S. Bagus, A. Schertel, T. Strunskus, M. Grunze, and Ch. Wöll, *Surf. Sci. Lett.* **341**, L1055 (1995).
- ³⁷D. N. Futaba and S. Chiang, *Jpn. J. Appl. Phys., Part 1* **38**, 3809 (1999).
- ³⁸O. Gröning and R. Fasel, *STM Generator Software* (EMPA Materials Science and Technology, Switzerland, 2004).
- ³⁹J. K. Fremerey, *Vacuum* **53**, 197 (1999).